International Journal of Thermophysics, Vol. 23, No. 1, January 2002 (© 2002)

Thermophysical Property Measurements on Niobium and Titanium by a Microsecond-Resolution Pulse-Heating Technique Using High-Speed Laser Polarimetry and Radiation Thermometry[1]

K. Boboridis[2, 3]

A microsecond-resolution technique was used to measure the heat of fusion, specific heat capacity, and electrical resistivity of niobium and titanium in the temperature range of 1600 to 3200 and 1500 to 2200 K, respectively. The method is based on rapid resistive self-heating of a wire-shaped specimen by a current pulse from a capacitor–discharge system. Melting of the specimen occurs in approximately 50 μs. Measured quantities are the current through the specimen, the voltage across the specimen, the radiance from the specimen, and its normal spectral emittance, as functions of time. The true temperature of the specimen is computed from the values of the normal spectral emittance and radiance temperature of the specimen at each instant. The latter quantities are measured by means of high-speed laser polarimetry and radiation thermometry, respectively.

KEY WORDS: electrical resistivity; emittance; heat of fusion; high temperatures; liquid metals; melting; niobium; pulse heating; refractory metals; titanium; transient techniques.

1. INTRODUCTION

This paper describes measurements on niobium and titanium using a microsecond-resolution dynamic technique. The method is based on rapid resistive self-heating of a wire-shaped specimen by a current pulse from a

[1] Paper presented at the Fourteenth Symposium on Thermophysical Properties, June 25–30, 2000, Boulder, Colorado, U.S.A.

[2] Guest Scientist from the Institut für Experimentalphysik, Technische Universität Graz, Petersgasse 16, A-8010 Graz, Austria.

[3] To whom correspondence should be addressed at Metallurgy Division, National Institute of Standards and Technology, Gaithersburg, Maryland 20899, U.S.A. E-mail: bobo@lanl.gov

0195-928X/02/0100-0277/0 © 2002 Plenum Publishing Corporation

capacitor-discharge system. Due to the high heating rate, more than 10^7 $K \cdot s^{-1}$, the cylindrical geometry of the specimen is preserved into the liquid state, up to temperatures hundreds of degrees above the melting point. In addition, because of the very short duration of the experiments (less than 100 μs), problems such as chemical reactions and evaporation that arise in conventional steady-state and quasi-steady-state property measurements at elevated temperatures are negligible. The measured quantities include the current through the specimen, the voltage across the specimen, the radiance from the specimen, and its normal spectral emittance. A high-speed single-wavelength pyrometer is used to measure radiance. The normal spectral emittance at a wavelength close to the pyrometer's operating wavelength is measured using a high-speed laser polarimeter.

2. MEASUREMENT SYSTEM

Details regarding the construction and operation of the capacitor–discharge circuit, including the current and voltage measurement, are given elsewhere [1, 2]. Additions to the existing system included a new vacuum chamber and provisions to accommodate a microsecond-resolution laser polarimeter for normal spectral emittance measurements.

2.1. Division-of-Amplitude Photopolarimeter (DOAP)

The DOAP consists of three modules: the polarization state generator (PSG), the polarization state detector (PSD), and the electronics module. To minimize problems associated with the high level of electromagnetic noise generated during the capacitor discharge, the electronics module is located outside the shielded room that encloses the discharge circuit. It contains a modulated laser diode operating at 677 nm and four high-speed photodiodes, each with its own amplification and demodulation electronics. The laser light is delivered to the PSG, which is located inside the shielded room and close to the experiment chamber, with a fiber-optic cable. The PSG contains a linear polarizer, a quarter-wave-retarder (QWR), a pair of computer-controlled motors to rotate these components to generate the desired state of polarization for the incident laser light, and a lens to focus the laser beam on the specimen. Light reflected from the specimen is collected by the PSD, which is also located close to the experiment chamber. The angle between the incident beam and the reflected beam entering the PSD is 140°. The PSD consists of an iris diaphragm, a narrow-bandwidth interference filter at the laser wavelength, an objective lens that focuses the collected light onto a small aperture, a collimating lens, a coated beam splitter, two beam-splitting Glan–Thompson prisms,

and a CCD camera for alignment purposes. The output of the PSD consists of four light signals that are delivered to the electronics module outside the shielded room via four fiber-optic cables. More details regarding the construction, operation, and calibration of the DOAP are given in Ref. 3.

2.2. Radiometric System

The radiance temperature of the pulse-heated specimens was measured using a single-wavelength high-speed pyrometer operating at 656.3 nm with a FWHM bandwidth of 30 nm. The pyrometer has low-gain and high-gain outputs. The nominal radiance temperature ranges for the two outputs are 1500 to 2800 and 1400 to 2200 K, respectively. The target viewed on the specimen was a rectangular area of 9.8×0.5 mm.

The pyrometer was calibrated prior to the measurements against a tungsten-filament reference lamp, which, in turn, had been calibrated against the NIST Photoelectric Pyrometer by the Optical Technology Division at NIST. All temperatures reported in this paper are based on the International Temperature Scale of 1990 (ITS-90) [4].

3. EXPERIMENTS

The specimens were in the form of wires with a nominal diameter of 1.6 mm and a nominal length of 50 mm. Each specimen was weighed using a precision scale, and its length was measured using a traveling microscope to determine its linear density (mass per length). It was then clamped into the experiment chamber, with approximately 38 mm of the specimen exposed between the clamps. Knife marks were made on the middle portion of each specimen approximately 23 mm apart. These marks defined an "effective length" across which the voltage was measured. This effective length was measured using the traveling microscope. Tantalum strips (6.4 mm wide and 0.25 mm thick) that were sharpened to a knife-edge on one end were placed on the knife marks to serve as voltage probes with the sharp end touching the specimen. Some tension was applied to the voltage probes to ensure good electrical contact. Prior to each measurement, the experiment chamber was first evacuated and then filled with an inert gas to slightly above atmospheric pressure. Also prior to each measurement, one to three capacitor discharges were performed, to adjust a tuning coil and bring the measured voltage in phase with the measured current, as described in Ref. 2. To limit the heating of the specimen caused by these "phase-matching" trials, the capacitor bank was only charged to a low voltage.

3.1. Measurements on Niobium

The purity of the niobium material was 99.9+%. The impurities as reported by the manufacturer were as follows: Ta, 100 ppm; O, 73 ppm; W, 50 ppm; N, 29 ppm; Zr, Mo, Ti, Fe, Ni, Si, Mn, Ca, Al, Cu, Sn, Cr, V, Co, Mg, Pb, and Hf, each less than 20 ppm; and C, H, B, and Cd, together less than 21 ppm.

Measurements were made on a total of 19 niobium specimens. Some of them were used "as received," some were treated with fine abrasive paper, some were subjected to one or two "preheating" pulses from a battery bank prior to the experiments, and some of the specimens were both treated with abrasive paper and preheated. These preheating pulses were about 250 ms in duration and heated the specimen to a set radiance temperature in the range of 1750 to 2000 K, which corresponded to a range in true temperature of approximately 1880 to 2170 K. This was done in an effort to remove oxides from the surface and to improve the specular reflectivity of the specimens for the laser-polarimetric measurement of emittance.

The capacitor bank was charged to an initial voltage of 6.6 to 6.7 kV and discharged in the crowbar mode of operation [2]. The specimen was heated from room temperature to its melting point in approximately 50 μs. The peak current through the specimen was about 45 kA, and the peak voltage across its effective length was close to 275 V. The heating rate in the solid phase at about 200 K below the melting point was approximately 5×10^7 K·s^{-1}.

3.2. Measurements on Titanium

As reported by the manufacturer, the titanium material was 99.9% pure, with the following major impurities: O, 700 ppm; Fe, 300 ppm; C, 100 ppm; N, 40 ppm; and H, 35 ppm.

Measurements were made on seven titanium specimens. Some of the specimens were treated with abrasive paper prior to the experiments. In a typical experiment, the capacitor bank was charged to 4.3 kV and discharged in the crowbar mode of operation [2]. The peak current through the specimen was about 25 kA, and the peak voltage across its effective length was approximately 500 V. The melting point was reached in about 40 μs. The heating rate in the solid phase at about 200 K below melting was approximately 6.5×10^7 K·s^{-1}. The $\alpha \rightarrow \beta$ phase transformation of titanium at 1166 K [5], which is accompanied by a rapid resistance change, was visible as a sudden change in the slope of the voltage trace.

4. DATA REDUCTION

4.1. Normal Spectral Emittance

The polarization state of light can be characterized by the four Stokes parameters. To determine the normal spectral emittance of the pulse-heated specimen, the change in the polarization state of a laser beam upon reflection at the specimen was measured. Light reflected by the specimen was collected by the PSD and divided into four separate light beams whose intensities were measured. From the intensity vector $\mathbf{I} = [I_0\ I_1\ I_2\ I_3]^t$, where t stands for the transpose, and the instrument calibration matrix $\mathbf{F}$, the Stokes vector $\mathbf{S_r} = [S_{r,0}\ S_{r,1}\ S_{r,2}\ S_{r,3}]^t$ of the reflected light was obtained using:

$$\mathbf{S_r} = \mathbf{F}^{-1} \cdot \mathbf{I} \tag{1}$$

where $\mathbf{F}^{-1}$ stands for the inverse calibration matrix. $\mathbf{F}$ is a 4×4 real matrix that is determined by calibration. The calibration procedure is described in Refs. 6 and 7.

The ellipsometric angles ψ and Δ were then computed from the Stokes parameters of the incident and reflected laser light using:

$$\cos 2\psi = \frac{S_{r,1n} - S_{i,1n}}{S_{r,1n} \cdot S_{i,1n} - 1} \tag{2}$$

$$\sin \Delta = \frac{(1 - S_{i,1n} \cos 2\psi)(S_{r,2n} S_{i,3n} - S_{i,2n} S_{r,3n})}{(S_{i,2n}^2 + S_{i,3n}^2) \sin 2\psi} \tag{3}$$

$$\cos \Delta = \frac{(1 - S_{i,1n} \cos 2\psi)(S_{r,2n} S_{i,2n} + S_{r,3n} S_{i,3n})}{(S_{i,2n}^2 + S_{i,3n}^2) \sin 2\psi} \tag{4}$$

The subscript i stands for "incident" and the subscript r stands for "reflected." The letter n in the subscript indicates that the Stokes parameters in the above equations are normalized with respect to S_0. For the work presented here, linearly polarized incident light of $+45$ and of $+135°$ azimuth with respect to the plane of incidence was used. In the former case, the Stokes parameters of the incident light were $S_{i,1n} = 0$, $S_{i,2n} = 1$, and $S_{i,3n} = 0$, and in the latter case $S_{i,1n} = 0$, $S_{i,2n} = -1$, and $S_{i,3n} = 0$.

From the ellipsometric angles and the angle of incidence $\Theta = 70°$, the refractive index n and the extinction coefficient k of the specimen were derived using

$$n - jk = n_0 \tan \theta \left[1 - \frac{4q \sin^2 \theta}{(1+q)^2} \right]^{\frac{1}{2}} \tag{5}$$

where $q = \tan\psi e^{j\Delta}$, $n_0 = 1.00028$ is the refractive index of the transparent ambient medium, and $j = \sqrt{-1}$ [8]. In the next step the normal spectral reflectance R_λ was computed from n and k:

$$R_\lambda = \frac{(n-n_0)^2+k^2}{(n+n_0)^2+k^2} \tag{6}$$

Finally, from the energy balance for opaque materials (incident light = reflected light + absorbed light) and Kirchhoff's law, the normal spectral emittance ε_λ was obtained:

$$\varepsilon_\lambda = 1 - R_\lambda \tag{7}$$

4.2. Temperature

The specimen radiance temperature T_r at each instant was obtained from the pyrometer output signal S using

$$T_r = \frac{c_2}{n_0\lambda \ln((b/S)+1)} \tag{8}$$

and the true temperature T of the specimen was derived from the radiance temperature T_r and the normal spectral emittance ε_λ using

$$T = \frac{c_2}{n_0\lambda \ln\{\varepsilon_\lambda[\exp(c_2/n_0\lambda T_r)-1]+1\}} \tag{9}$$

where b is a constant determined by calibration, $c_2 = 0.014388$ m·K is the second radiation constant, and $\lambda = 656.3$ nm. No correction was applied to account for the difference between the wavelength at which the radiance temperature and that at which the normal spectral emittance were measured. Also, no correction was applied to account for the small shift with temperature of the effective wavelength of the pyrometer.

4.3. Resistivity[4]

The specimen resistivity at each instant was determined from the measured voltage V across the "effective" specimen length l_{eff} and the measured current I through the specimen:

$$\rho = \frac{V}{I}\frac{\gamma_{\text{lin}}}{\gamma l_{\text{eff}}} \tag{10}$$

[4] The electrical resistivity data presented in this paper are based on the room-temperature specimen dimensions and are not corrected for thermal expansion.

where γ_{lin} is the linear density of the specimen (mass per length) and γ is the density of the specimen. For niobium, $\gamma = 8.57\ \text{g}\cdot\text{cm}^{-3}$ and, for titanium, $\gamma = 4.54\ \text{g}\cdot\text{cm}^{-3}$ was used. The linear density of each individual specimen was determined prior to the experiment so that small differences in the specimen diameter, caused by different degrees of polishing, could be taken into account. The average value of γ_{lin} for the niobium specimens was $0.1682\ \text{g}\cdot\text{cm}^{-1}$, and that for the titanium specimens was $0.08490\ \text{g}\cdot\text{cm}^{-1}$.

Equation (10) implicitly assumes a uniform temperature distribution in the specimen at each instant during heating. The contribution of conduction, convection, and even radiation to the establishment of temperature gradients (longitudinal and/or radial) in the "effective" specimen was negligible because of the temperatures and heating rates involved in these measurements. In addition, under the operational conditions of the present work, the skin effect was insignificant [1].

For each experiment the true temperature was plotted against the resistivity. A plateau indicated melting of the specimen. Linear functions were fitted to the data in the solid phase and in the liquid phase. Using these fits, the resistivity was computed every 50 K in the temperature range of interest. The computed resistivity values from all experiments were then plotted versus the temperature in a single graph and linear functions were fitted to these data to obtain Eqs. (12) and (14).

In the case of niobium a linear function was also fitted to the data in the melting plateau of each experiment. The intersections of the melting-plateau fit with the solid-phase fit and with the liquid-phase fit provided the resistivity values at the start and at the end of melting, respectively. In the case of titanium, however, resistivity changed only little during melting. Fitting a straight line to such a short melting plateau (in terms of resistivity change) was impractical. To obtain the resistivity of titanium at the start and at the end of melting, the solid- and liquid-phase fits were extrapolated to the average temperature of the melting plateau instead.

4.4. Heat of Fusion

The specific energy absorbed by the specimen during heating as a function of time was computed as the integral of imparted electrical power over time, divided by the number of moles of the "effective" specimen:

$$\Delta q(t) = \frac{M}{\gamma_{\text{lin}} l_{\text{eff}}} \int_0^t V(t')\, I(t')\, dt' \tag{11}$$

where M is the molar mass of the specimen material. For niobium, $M = 92.91$ and, for titanium, $M = 47.88$ was used. To obtain the heat of

fusion, the temperature was plotted as a function of Δq. A plateau in that plot indicated melting of the specimen. For niobium a quadratic function was fitted to the solid-phase data and linear functions were fitted to the melting plateau and to the data in the liquid phase. For titanium linear functions were fitted to the data in the solid phase, the melting plateau, and in the liquid phase. The intersections of these three fits defined the beginning and the end of melting. The heat of fusion h_F was then computed as the difference between the value of the absorbed energy Δq at the end of the melting plateau and that of the absorbed energy at the beginning of the melting plateau.

4.5. Specific Heat Capacity

For an isobaric experiment the increase in the specific enthalpy $h(t)$ of the specimen is equal to the electrical energy $\Delta q(t)$ absorbed by it during heating. Therefore, the plots of temperature vs absorbed energy, which were used to obtain the heat of fusion, are at the same time plots of temperature vs specific enthalpy. The specific heat capacity $c_p(T)$, which is equal to the derivative of the specific enthalpy with respect to temperature $dh(T)/dT$, was computed as the reciprocal of the slope dT/dh of the functions that were fitted to the temperature-vs-absorbed energy data.

In computing the specific heat capacity, no correction was necessary to account for heat losses. At the temperatures and speeds involved in the present work, the only significant heat loss from the specimen can be that due to thermal radiation. For the specimen geometry that was used in this work, the radiative heat losses were estimated via the Stefan–Boltzmann law to be less than 0.02% of the imparted electrical power and were, thus, negligible.

5. RESULTS

5.1. Niobium

The mean value of the true temperature at the melting transition of niobium was 2736 K. The standard deviation from the mean was 25 K. The normal spectral emittance exhibited a rapid decrease at melting, and remained constant in the liquid phase, up to 3200 K. Its mean value in the liquid phase was 0.36 (at 677 nm). The standard deviation from the mean was 0.026. For a given specimen, the melting temperature (radiance or thermodynamic) was determined by averaging the measured temperatures (data points) along the melting plateau. The standard deviation of an individual temperature from the plateau average was in the range of 0.1 to

2.7 K for the radiance temperature plateaus and in the range of 11 to 29 K for the true temperature plateaus. The trend of radiance and thermodynamic temperature along each plateau was determined by (least-squares) fitting a linear function of time to the measured temperatures. The slope of the radiance temperature plateaus was in the range of 0.038 to 0.664 $K \cdot \mu s^{-1}$, and that of the true temperature plateaus in the range of -0.765 to 3.3 $K \cdot \mu s^{-1}$.

The linear functions representing the resistivity ρ of solid and liquid niobium in the temperature ranges of 1600 to 2700 and 2800 to 3200 K, respectively, were

$$\begin{aligned} &\text{Solid:} && \rho = 60.8 + 2.42 \times 10^{-2} (T - 1600) \\ &\text{Liquid:} && \rho = 98.7 + 3.95 \times 10^{-3} (T - 2800) \end{aligned} \tag{12}$$

where T is in $\mu\Omega \cdot cm$ and T is in K. Equation (12) is plotted in Fig. 1. The mean values of the resistivities at the beginning and at the end of melting were 87.5 and 98.5 $\mu\Omega \cdot cm$, respectively.

The mean value that was obtained for the heat of fusion of niobium was 32.0 $kJ \cdot mol^{-1}$. The standard deviation from the mean was 1.5 $kJ \cdot mol^{-1}$.

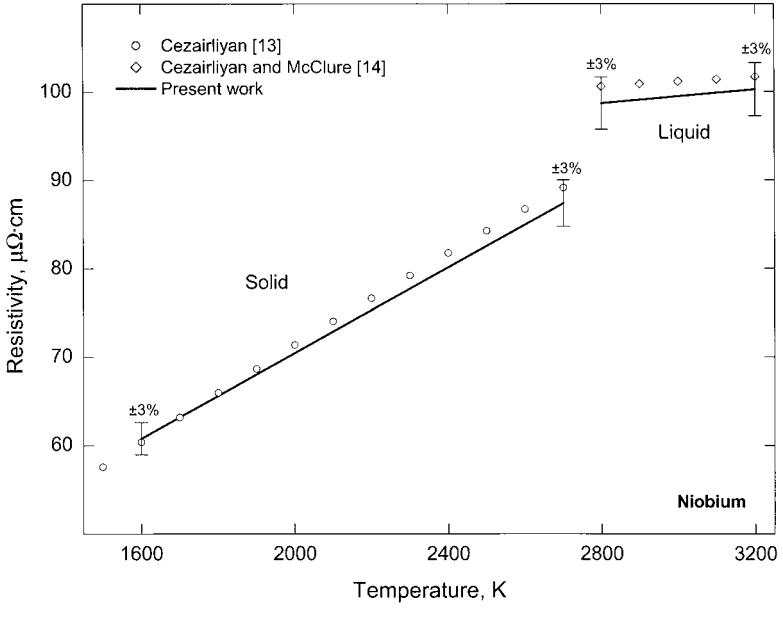

Fig. 1. Electrical resistivity of niobium as a function of temperature.

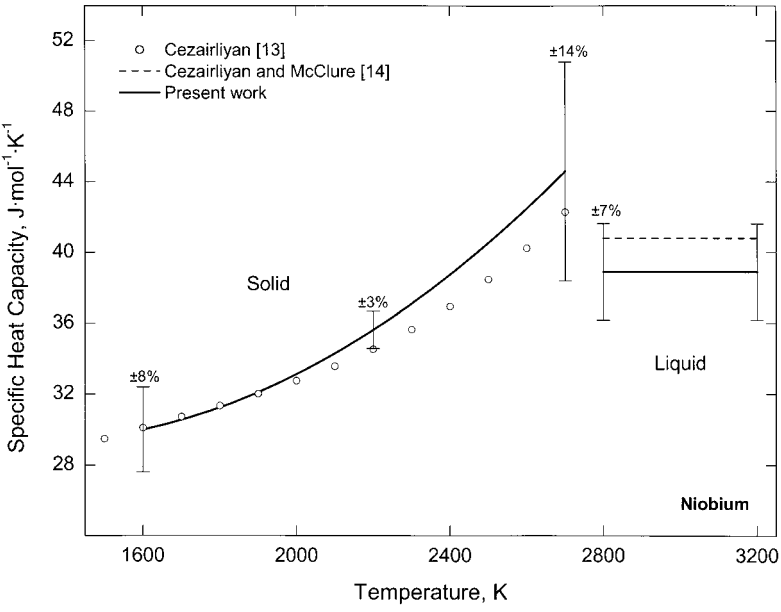

Fig. 2. Specific heat capacity of niobium as a function of temperature.

The quadratic function that was fitted to the specific heat capacity data of solid niobium in the range of 1600 to 2700 K was

$$c_p = 30.0 + 4.7 \times 10^{-3} (T - 1600) + 7.8 \times 10^{-6} (T - 1600)^2 \qquad (13)$$

where c_p is in $J \cdot mol^{-1} \cdot K^{-1}$ and T is in K. Equation (13) is plotted in Fig. 2. In the liquid phase a linear increase in the specific enthalpy with temperature was observed, yielding a constant value of 38.9 $J \cdot mol^{-1} \cdot K^{-1}$ for the specific heat capacity of liquid niobium up to 3200 K.

5.2. Titanium

The mean value of the true temperature at the melting transition of titanium was 1941 K. The standard deviation from the mean was 6 K. The mean value of the normal spectral emittance (at 677 nm) at the melting point of titanium was 0.52. The standard deviation from the mean was 0.03. For any given specimen, the standard deviation of an individual temperature (data point) on the melting plateau from the plateau average was in the range of 0.75 to 1.9 K for the radiance temperature plateaus and in the range of 5.9 to 10 K for the true temperature plateaus. The slope of the radiance temperature plateaus was in the range of -0.14 to 0.8 $K \cdot \mu s^{-1}$,

and that of the true temperature plateaus was in the range of -1.0 to 2.3 $K \cdot \mu s^{-1}$.

The linear functions representing the resistivity ρ of solid titanium in the temperature range of 1500 to 1900 K and of liquid titanium in the range of 1950 to 2200 K were

$$\begin{aligned} &\text{Solid:} \quad \rho = 149.6 + 1.57 \times 10^{-2} (T - 1500) \\ &\text{Liquid:} \quad \rho = 156.9 - 6.48 \times 10^{-3} (T - 1950) \end{aligned} \tag{14}$$

where ρ is in $\mu\Omega \cdot cm$ and T is in K. Equation (14) is plotted in Fig. 3. At the beginning and at the end of melting, the mean values of the measured resistivities were 156.5 and 157.0 $\mu\Omega \cdot cm$, respectively.

The mean value of the heat of fusion of titanium from all experiments was 13.2 $kJ \cdot mol^{-1}$. The standard deviation from the mean was 0.4 $kJ \cdot mol^{-1}$.

For the specific heat capacity of titanium in the temperature ranges of 1500 to 1900 K (solid) and of 1950 to 2200 K (liquid), constant values of 37.6 and 35.3 $J \cdot mol^{-1} \cdot K^{-1}$, respectively, were obtained (see Fig. 4). Although it is common for liquid metals to have a constant heat capacity, a constant value in the solid phase is not realistic. The reason for not being able to resolve a positive (upward) curvature in the specific enthalpy-vs-

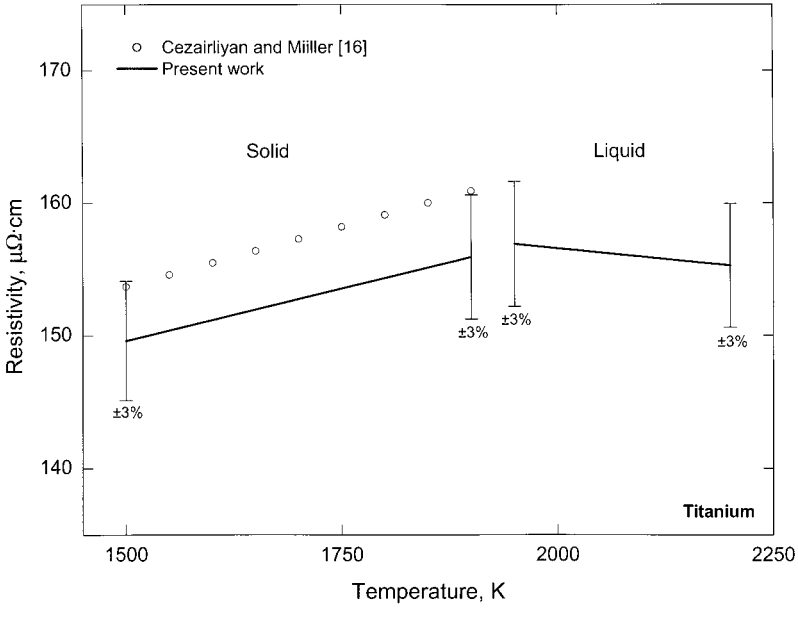

Fig. 3. Electrical resistivity of titanium as a function of temperature.

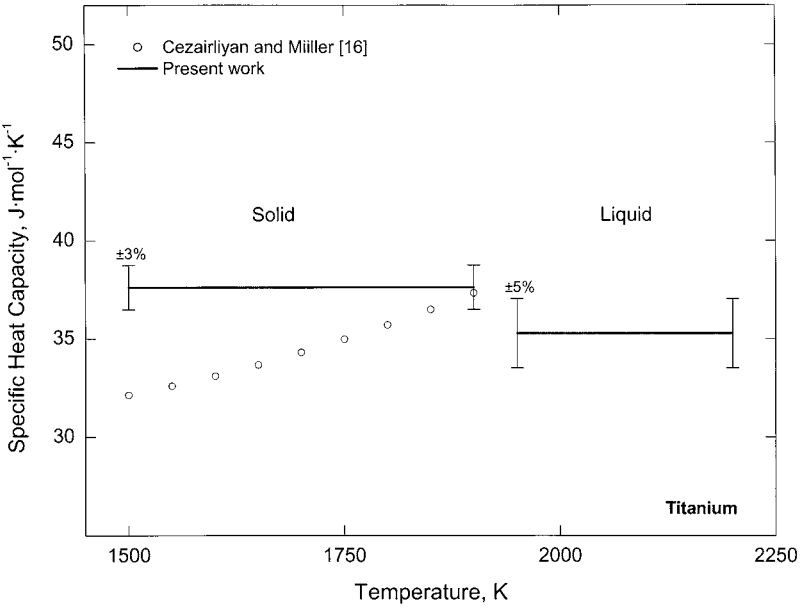

Fig. 4. Specific heat capacity of titanium as a function of temperature.

temperature data, which would have led to an increasing heat capacity with temperature, was the noise in the computed true temperature[5] combined with the short temperature interval that was covered in the solid.

6. ESTIMATE OF UNCERTAINTIES

Uncertainties reported here are expanded uncertainties with a coverage factor $k = 2$, and thus, they are 2-standard deviation estimates [9]. A detailed discussion of uncertainties associated with the measurement of current and voltage is given in Ref. 2. Uncertainties associated with the temperature measurement are discussed in Refs. 10 and 11. Specific items in the error analysis were recomputed when the present conditions differed from those in the earlier publications.

The uncertainty in the reported melting temperatures is ± 25 K for niobium and ± 13 K for titanium. The uncertainty in the reported resistivity values is $\pm 3\%$. The uncertainty in the reported heat of fusion is $\pm 5\%$ for niobium and $\pm 7\%$ for titanium. The uncertainty in the specific heat capacity of solid niobium is $\pm 8\%$ at 1600 K, decreases to $\pm 3\%$ at 2200 K, and

[5] At the low end of the pyrometer's useful temperature range, this noise is mainly digitization noise in the measured radiance.

increases again to ±14% at 2700 K (see Fig. 2). In the liquid phase the uncertainty is ±7%. For titanium, the uncertainty in the reported specific heat capacity is ±3% in the solid phase and ±5% in the liquid phase.

7. DISCUSSION

True temperature measurements at the microsecond-resolution pulse-heating facility at NIST were made possible for the first time with the addition of the division-of-amplitude photopolarimeter. In the past, lack of information on the normal spectral emittance of the specimens rendered the determination of true temperature in the solid phase impossible. In the liquid phase the true temperature could be obtained from radiance temperature only when the melting temperature of the specimen was known, and then under the assumption that the emittance above melting did not deviate from its value at the melting point.

The scope of this work was to validate the laser-polarimetric technique for the measurement of normal spectral emittance of pulse-heated specimens in the microsecond-resolution regime. A comparison between the property data presented here with results obtained previously at NIST, using the millisecond- and microsecond-resolution pulse-heating facilities, generally showed a good agreement [12–17]. The exception was the specific heat capacity of solid titanium, particularly at the lower temperatures, where the deviation from previous data is significant (see Section 5.2 and Fig. 4).

An interesting finding of this work was that the radiance temperature at the melting point of niobium showed a dependence on the treatment that each specimen received prior to the experiment. Specimens that were used "as received" or were treated with abrasive paper melted at a higher radiance temperature than specimens that were preheated prior to the experiment and those that were first treated with abrasive paper and then preheated. The differences, which in some cases amounted to more than 15 K, are believed to be the result of different values of emittance at the melting point, caused by different degrees of surface roughness. This is a major difference from slower pulse-heating experiments, where it has been shown [18] that the radiance temperature at the melting point is constant, regardless of the treatment given to the specimen prior to the experiment, probably because there is enough time for the surface to become smooth. The trend in the measured emittances at the melting point of the differently treated niobium specimens used in this work agreed with the observed behavior of the melting-point radiance temperature. Unfortunately, the low signal-to-noise ratio of the polarimeter that was used in the present work resulted in a large standard deviation of the measured emittance among

specimens that had received the same treatment, so that the difference between specimens that had received different treatments, though in the right direction, was not statistically significant.

In the case of titanium, the normal spectral emittance at the melting point was about 30% higher than the value measured in the past using the millisecond-resolution pulse-heating facility at NIST [15]. At the same time, the melting-point radiance temperature was also higher, so that the computed true temperature was very close to that reported in Ref. 15. Furthermore, it was observed that the normal spectral emittance of titanium dropped later in the liquid phase to a value close to the one measured in the slower system at the melting point. This supports the theory that in the faster experiments there is not enough time for the surface to become smooth during melting. It also emphasizes the need for *in situ* measurements of the normal spectral emittance. Using the known melting (true) temperature of titanium to calibrate the radiance temperature trace and assuming constant emittance in the liquid phase, as was routinely done in the past, would have resulted in large errors in the temperature measurement. Further research in this area should prove very informative and valuable.

ACKNOWLEDGMENT

This work was supported in part by the Microgravity Science and Applications Division of NASA.

REFERENCES

1. A. Cezairliyan and J. L. McClure, *Int. J. Thermophys.* **8**:577 (1987).
2. J. L. McClure and A. Cezairliyan, *Int. J. Thermophys.* **11**:739 (1990).
3. S. Krishnan and K. Boboridis, *Rev. Sci. Instrum.* (in preparation).
4. H. Preston-Thomas, *Metrologia* **27**:3 (1990), **27**:107 (1990).
5. A. Cezairliyan and A. P. Miiller, *J. Res. Natl. Bur. Stand.* **83**:127 (1978).
6. R. M. A. Azzam and A. G. Lopez, *J. Opt. Soc. Am. A* **6**:1513 (1989).
7. S. Krishnan, *J. Opt. Soc. Am. A* **9**:1615 (1992).
8. R. M. A. Azzam and N. M. Bashara, *Ellipsometry and Polarized Light* (North-Holland, Amsterdam, 1987), p. 274.
9. B. N. Taylor and C. E. Kuyatt, *Guidelines for Evaluating and Expressing the Uncertainty of NIST Measurement Results*, NIST Technical Note 1297 (1994).
10. A. Cezairliyan and A. P. Miiller, *Int. J. Thermophys.* **13**:39 (1992).
11. A. Cezairliyan, G. M. Foley, M. S. Morse, and A. P. Miiller, in *Temperature: Its Measurement and Control in Science and Industry, Vol. 6, Part 2* (AIP, New York, 1992), p. 757.
12. A. Cezairliyan, *High Temp. High Press.* **4**:453 (1972).
13. A. Cezairliyan, *J. Res. Natl. Bur. Stand.* **75A**:565 (1971).

14. A. Cezairliyan and J. L. McClure, *Int. J. Thermophys.* **8**:803 (1987).
15. A. Cezairliyan and A. P. Miiller, *J. Res. Natl. Bur. Stand.* **82**:119 (1977).
16. A. Cezairliyan and A. P. Miiller, *High Temp. High Press.* **9**:319 (1977).
17. J. L. McClure and A. Cezairliyan, *Int. J. Thermophys.* **13**:75 (1992).
18. A. Cezairliyan, A. P. Miiller, F. Righini, and A. Rosso, in *Temperature: Its Measurement and Control in Science and Industry, Vol. 5, Part 1* (AIP, New York, 1982), p. 377.